Thin Film Oxide Barrier Layers: Protection of Kapton from Space Environment by Liquid Phase Deposition of Titanium Oxide

Irina Gouzman,*,† Olga Girshevitz,‡ Eitan Grossman,† Noam Eliaz,§ and Chaim N. Sukenik‡

Space Environment Section, Soreq NRC, Yavne 81800, Israel, Department of Chemistry and Institute for Nanotechnology and Advanced Materials, Bar-Ilan University, Ramat Gan 52900, Israel, and School of Mechanical Engineering and the Materials and Nanotechnologies Program, Tel-Aviv University, Ramat Aviv, Tel-Aviv 69978, Israel

ABSTRACT Polyimides are widely used for the external surfaces of spacecraft. In low Earth orbit (LEO), they are exposed to atomic oxygen (AO) and to problems of electrostatic discharge (ESD). This work demonstrates that liquid-phase deposition (LPD) of titania creates a protective coating on Kapton polyimide that is effective in reducing AO-induced surface erosion and in preventing ESD. Adherent titania coatings, 100−300 nm thick, were deposited on Kapton at near-ambient conditions by LPD using an aqueous solution of a metal-fluoride complex and boric acid. Characterization of the oxide-coated Kapton included atomic force microscopy (AFM) in tapping and nanoindentation modes, electrostatic force microscopy (EFM), scanning electron microscopy (SEM), Rutherford backscattering (RBS) and X-ray photoelectron spectroscopy (XPS). The as-deposited titania-coated Kapton can be prepared without significant changes in the original thermo-optical properties of the polymer, while preventing ESD and improving the surface hardness. The durability of the oxide coating under AO attack was studied using an oxygen RF plasma. Surface erosion was measured both gravimetrically and by in situ quartz crystal microbalance (QCM) measurements. The AO exposure caused some changes in the thermo-optical properties and surface morphology. The erosion yield of titania-coated Kapton was only 2% of that observed for uncoated Kapton after exposure to 4×10^{20} O-atoms cm^{-2} of LEO equivalent AO fluence.

KEYWORDS: atomic oxygen • space environment • titania • liquid-phase deposition

1. INTRODUCTION

Polyimide films are widely used onboard spacecraft, mainly as external thermal blankets (1), thus they are exposed extensively to the space environment. The low Earth orbit (LEO) space environment presents many obstacles to a successful spacecraft mission. The degrading environment for polymers includes atomic oxygen (AO), ultraviolet (UV) and ionizing radiation, ultrahigh vacuum (UHV), thermal cycles, micrometeoroids, and orbital debris (2, 3). AO, produced by the photodissociation of molecular oxygen in the upper atmosphere, is the main constituent of the residual neutral atmosphere in LEO (4) and is one of the most serious hazards to the spacecraft exterior. Hyperthermal AO reacts with polymers and any other carbon-based materials and causes surface erosion. The erosion yield of Kapton H has been measured by numerous in-flight and ground simulation tests and the agreed upon value is 3×10^{-24} cm^3 $atom^{-1}$ (5, 6). This value is generally used as a standard for AO fluence measurements in ground-based simulation facilities (5).

Various approaches have been developed to improve the space survivability of polyimides. The different protective strategies may be divided into three categories: (a) application of protective, mainly oxide, coatings produced by different methods (7, 8); (b) surface modification (e.g., by ion implantation or by direct application of siloxanes) (9–11); and (c) development of advanced materials that are inherently stable under oxidizing environment. An example of such materials is the POSS/polyimide nanocomposite (12, 13). Each of these approaches has both advantages and drawbacks.

The most common method is to use inorganic coatings, such as SiO_2 (14), that physically block the interaction of oxygen with the polymer. In an orbit characterized by a high flux of charged particles (e.g., polar orbit), the protective inorganic coatings are not sufficient. Spacecraft orbiting in such an environment also require coatings with suitable antistatic properties, such as tin-doped indium oxide (ITO) (15), so as to protect from electrostatic discharge (ESD).

Progress in the application of ceramic thin-film coatings has included advances in film deposition technologies such as plasma enhanced chemical vapor deposition (PE-CVD), sputtering, laser ablation, and evaporation (16). These techniques, however, have considerable shortcomings: the equipment costs can be prohibitively high; they are often line-of-sight limited (9–11); and an elevated temperature is usually required to convert the as-deposited materials into crystalline films (17). Finally, there is a recent report using atomic layer deposition (ALD) of Al_2O_3 films (18, 19). This method is a variation of CVD based on subjecting substrates to chemically reactive vapors that grow thin surface films in a

* Corresponding author.
Received for review February 7, 2010 and accepted June 5, 2010
† Soreq NRC.
‡ Bar-Ilan University.
§ Tel-Aviv University.
DOI: 10.1021/am100113t

self-limiting fashion. Although it demands carefully controlled exposure times and pressures, it does not rely on line-of-sight deposition and does not require high surface temperatures. It holds significant promise for polymer protection.

Liquid phase deposition (LPD) is an alternative strategy for the preparation of ceramic films. It is technologically simpler since it involves film deposition from aqueous solution under near-ambient conditions. LPD generally refers to the formation of oxide films from an aqueous solution of a metal-fluoride complex ($[TiF_6]^{2-}$) which is slowly hydrolyzed in water and boric acid. This technique is not line-of-sight limited and allows coating of substrates with complex shapes. It was initially developed to deposit thin ceramic films on glass, or on silicon (20, 21). Work from one of our laboratories has studied LPD of titania films on Si wafers with and without various self-assembled monolayers (SAM) and then adapted these methods to coating polyimides (PMR-15 and BMI) (22–24). Titanium dioxide has important optical and electronic properties, and is used in gas-sensing devices and antireflection coatings for solar-cells and deep ultraviolet (UV) lithography (25–27). Because titanium dioxide is a wide band gap semiconductor ($E_g = 3.25-3.33$ eV) (27, 28), it can potentially prevent ESD (2) and protect polymers from photodegradation. With an absorption coefficient of $\sim 1 \times 10^6$ cm^{-1} in the 200−300 nm range (29), a 100 nm thick titanium dioxide coating could almost completely (99%) block incident UV light in this range.

The present work extends previous studies by reporting the LPD of titania films on Kapton and studying the durability of this coating under AO attack. Titania-coated Kapton was thoroughly characterized in terms of its morphology, electrical, mechanical and thermo-optical properties. AO exposure was carried out in an RF plasma-based simulation facility, which allows both gravimetric and kinetic measurements of sample erosion.

2. EXPERIMENTAL DETAILS

2.1. Preparation of Titania-Coated Kapton. The studies were carried out on 125 μm thick Kapton 500 HN sheets (DuPont). Prior to titania coating, the as-received sheets were cut into squares (1.2 cm × 1.2 cm), washed with ultrapure water (resistivity 18 MΩ cm) and ethanol, and dried under nitrogen. The samples were then treated by one of the following three methods: (a) exposure to an air plasma (Harrick, model PDC-3XG) at a pressure of 0.3 mm Hg and 18 W power for 20 min; (b) treatment for 20 min in a UV Ozone cleaner (UVOCS); or (c) dipping into a solution of 20% H_2SO_4 in water for 15 min. Titania coatings were then applied.

LPD titania was deposited from a solution of a metal-fluoro complex ($[TiF_6]^{2-}$) as it slowly hydrolyzes in a mixture of water and boric acid. Two different LPD methods were used. Method I (20, 21) coatings were done from a pH 3.88 aqueous solution containing 0.3 M H_3BO_3 + 0.1 M $(NH_4)_2TiF_6$ at room temperature. Substrates were left in the solution for 8 h, after which they were washed with water and methanol and dried in a controlled humidity chamber (24, 30). Briefly, this involves keeping the samples at 80 °C, while the humidity was reduced from 80 to 60 to 40 to 20% over 50 h. The stepwise reduction of humidity under equilibrating conditions is crucial for the formation of crack-free films, 100−120 nm thick. Method II (31) coating solutions (pH 2.88; 0.15 M H_3BO_3 + 0.05 M $(NH_4)_2TiF_6$) were kept at 50 °C for 4 h. The coated samples were washed and dried as described above. The films formed in this way were 200−350 nm thick and showed occasional cracks even with the controlled humidity drying. Method I is a slower process and provides amorphous titania films. Method II deposits partially crystalline anatase films at a higher growth rate (30). Film thickness was determined by Rutherford back scattering (RBS) analysis and by cross-sectional SEM studies using a focused ion beam (FIB) to create the sample.

2.2. Characterization Methods. The morphology, mechanical and electrostatic properties of titania-coated Kapton before and after exposure to simulated space environment were studied using an atomic force microscope (AFM, Nanoscope IV MultiMode from Veeco). The measurements were carried out in tapping, nanoindentation/scratching and electrostatic modes, respectively. Mechanical properties were measured using a diamond-tipped cantilever made by Veeco (model DNISP) with a Berkovich indenter of about 50 nm tip radius. Nanoindentation was performed with a tip load of 5 to 50 μN. Nanoscratching was done with the indenter at a normal load of 6 μN, a sliding speed of 2 μm/s and a scratch length of 3 μm. The same indenter was used to scan the area after the nanomechanical tests. Electrostatic properties of the coating were assessed by the Electrostatic Force Microscopy (EFM) module, using tip−surface distances of 25−100 nm with an applied voltage of 0−5 V. The EFM mode used silicon tips coated with a thin film of CoCr (Model MESP, Veeco, Inc.).

The surface morphology was studied using a Quanta 200 Environmental SEM from FEI (ESEM). This microscope allows characterization of nonconductive samples without the need for a conductive coating.

The chemical composition of the surfaces was studied before and after titania deposition by X-ray photoelectron spectroscopy (XPS). XPS measurements were carried out using nonmonochromatized Al Kα radiation (1486.6 eV) and a hemispherical CLAM 2 (VG Microtech) analyzer. The binding energy scale was calibrated using an Ag($3d_{5/2}$) line at 368.3 eV as a reference. Pass energy of 100 eV was used for survey scans, while 20 eV pass energy was used for high-resolution measurements. Curve fitting of the core-level XPS lines was carried out using CasaXPS software (32).

Analysis of the titania-Kapton interface included XPS-depth profile and RBS analyses. The samples were analyzed by XPS (5600 Multi-Technique System, PHI, USA) during sputtering using 4 kV Ar^+ ion gun (sputter rate ~15.6 Å/min on SiO_2/Si). Surface charging was compensated by using a neutralizer. RBS studies were performed with a 2.0 MeV He^+ beam. The backscattered particles were detected using a silicon surface barrier detector with 30 keV resolution. The beam current was measured on the target and kept around

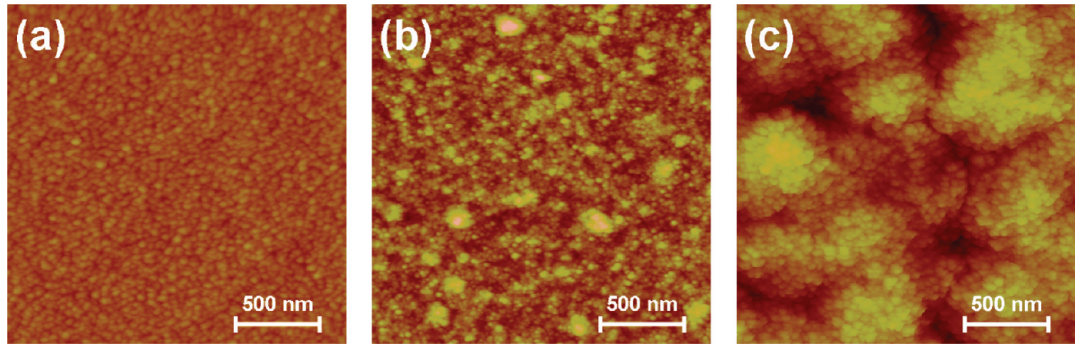

FIGURE 1. AFM images (2 × 2 μm) of (a) uncoated Kapton after air plasma pretreatment, and titania-coated Kapton prepared by (b) method I and (c) method II. Z-scale is 50 nm in (a) and (b), and 500 nm in (c).

13 nA. The RBS data was analyzed with RUMP software (33). Thermo-optical properties (α/ε) were measured using a Total Emmitance/Solar Absorbance (TESA 2000) portable reflectometer from AZ Technology, Inc.

2.3. Atomic Oxygen Exposure. The AO exposure facility is based on a LB-3000 Advanced Energy RF-plasma system with a feed gas of 99.999% pure oxygen. The system is operated at a pressure of 40 mTorr, power of 500 W, and oxygen flow of 10 sccm. Redirection of the afterglow through two right angle deflections results in a strong reduction of ion current and UV radiation flux, facilitated by a supply of electrons from the metallic chamber walls, and radiation absorption by the walls, respectively. The afterglow was characterized by optical emission spectroscopy (OES), electrical measurements, UV radiation measurements, and Kapton etching rate measurements. Detailed description of the AO simulation system is presented elsewhere (34). In the present work, the samples were exposed to the afterglow of the plasma, after one bend in the pumping system emerging from the plasma source. This position provides thermal AO with the addition of a UV radiation (115−200 nm) flux similar to that of space (about 90 mW/m^2, compared to 109 mW/m^2 in space), as well as some electronically excited species, ions, and electrons and molecular oxygen (34).

Atomic oxygen fluence measurements were conducted based on Kapton-HN mass loss, assuming an erosion yield of 2.81×10^{-24} cm^3 O-atom^{-1} and Kapton HN density 1.43 g/cm^3 (35). The erosion yield was determined gravimetrically, using an analytical balance (Mettler, model UM3) with an accuracy of ± 1 μg.

For kinetic measurements, polyimide films were spin-coated on quartz crystal microbalance (QCM) crystals using a Dupont procedure for deposition of polyimide (Pyralin PI 2545, HD MicroSystems) (36). The deposited polyimide films were shown to be similar to Kapton HN films based on their FTIR spectra (37). Titania coatings were deposited on Pyralin-coated QCM crystals.

3. RESULTS AND DISCUSSION

3.1. Surface Morphology. Figure 1 shows AFM images of air-plasma pretreated Kapton films and LPD of titania by method I and method II on air-plasma pretreated Kapton substrates. The surface morphology of uncoated Kapton (Figure 1a) is relatively smooth and uniform, with characteristic features of air plasma treatment and a surface roughness of R_q = 1.5 nm. Titania films deposited by method I (Figure 1b) show larger features and a slight increase in surface roughness to about 4.5 nm. Similar surface morphology, adhesion, and deposition rate were obtained for titania coating on Kapton substrates with different types of surface pretreatments (data not shown).

Titania films deposited by method II, however, showed a significant increase in surface roughness (from several nanometers to tens of nanometers). In this case, the film consists of "cauliflower"-shaped particles and the nucleation density, adhesion, and deposition rate depend on the surface pretreatment. More uniform, well-adhered films are produced on air plasma and UVOCS pretreated Kapton samples, as demonstrated in Figure 1c. Pretreatment by sulfuric acid was found to be less effective.

3.2. Titania/Kapton Interface Chemistry. XPS depth profiling was used to assess the interface structure and to verify the penetration of oxide into the polymer matrix. Figure 2 shows typical depth profile results for Ti, O and C atomic concentrations as a function of sputter depth for samples deposited by methods I and II. Film thickness, Z, and depth resolution (or interface width, ΔZ) are also indicated in the figure. It is observed that the interface width ΔZ is greater for samples produced by method II (reaching ~120 nm for the 190 nm thick film), whereas films produced by method I show an interface width of only 60 nm for a film thickness of 110 nm. The increase of the interface thickness, as measured by depth profile, might account for artifacts in the depth resolution due to nonuniform sputtering or knock-in effects. However, this factor was estimated to be negligible compared to the observed increase in the interface thickness, indicating interpenetration of TiO_2 into the Kapton substrate.

The thickness of titania films prepared by different methods and their penetration into the polymer were also measured by RBS (Table 1). ^{4}He with an energy of 2 MeV is used as the projectile and backscattering particles are detected by a simple Si detector. Our titania layers are thin enough so that the Ti, O and substrate signals are completely separated. For each element, the right-hand edge of the spectrum corresponds to the signal coming from the surface and the depth scale points to the left. The film thickness can

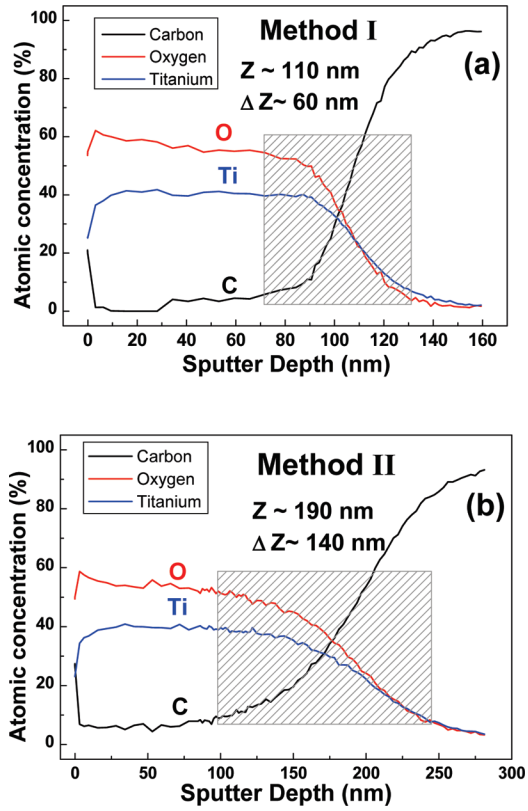

FIGURE 2. XPS depth profile results show the atomic concentration of Ti, O, and C as a function of sputter depth for titanium oxide films prepared by method I (a) and method II (b). Film thickness, Z, and depth resolution (or interface width, ΔZ) are indicated in the figure.

Table 1. Thickness of Titania Films Deposited by Different Methods, As Measured by RBS (nm)

substrate pretreatment	deposition method I			deposition method II		
	plasma	UVOCS	acid	plasma	UVOCS	acid
TiO_2	100	96	98	350	130	140
mixed TiO_2/Kapton				600	180	180

be calculated from the width of the box spectrum, which includes all species in the film, via the specific energy loss values in the material by semiempirical models with an accuracy of 3−5%, depending on the projectile-target atom combination. The density of amorphous titania (Method I) was estimated based on a previously calibrated sample to be 0.657×10^{23} atoms/cm^3 (23). The calibration was done by ellipsometry using titania deposited on a silicon wafer (23). The density thus obtained was used to calculate film thicknesses by RBS for all of the specimens produced by method I.

Representative RBS spectra of TiO_2-coated Kapton are shown in Figure 3. Superimposed red lines show the simulation results. The Ti and O peaks between channels 1000−1250 and 500−600, respectively, are due to the TiO_2 film on the surface of Kapton. Good agreement was obtained between the measured and simulated spectra in Figure 3a with a Ti:O ratio of 1:2, suggesting that the film was close to stoichiometric (Method I). The fluorine content in these films was 0.3%, as determined by the fit to the peak between channels 590−720, independent of the surface activation used. Figure

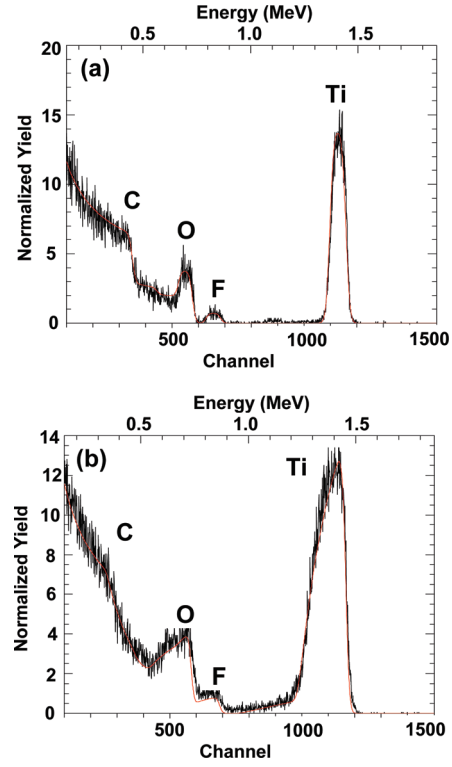

FIGURE 3. 2 MeV ^{4}He RBS spectra of the TiO_2 films deposited on Kapton by: (a) method I and (b) method II. Air plasma pretreatment was used in both cases. Red lines represent the RUMP simulated spectra.

3a also shows that the titania does not penetrate into the Kapton. This is reflected in the symmetry of both the titanium and oxygen peaks.

In method II, the thickness calculation was based on a density of bulk anatase of 0.868×10^{23} atoms/cm^3. The distribution of Ti and F in the film is not uniform. The percentage of these elements in the sample surface is relatively high and it decreases at greater sample depths. This is evident from the nonsymmetric Ti and O peaks between channels 950−1250 and 400−600, respectively (Figure 3b). Fitting of this region of the spectrum was accomplished by starting with the Kapton composition and progressively increasing the amount of TiO_2 and F, until reasonable agreement with the measured spectrum was obtained.

3.3. Atomic Oxygen Durability. Titania-coated Kapton samples (methods I and II) were subjected to AO exposure. The results presented below are for coatings prepared by Method I. Coatings prepared by method II showed similar results. The exposure time was varied so that AO fluences in the range of 4×10^{19} atoms cm^{-2} up to 2.5×10^{21} atoms cm^{-2} were achieved. The upper level is equivalent to exposure of a satellite external surface to LEO environment for approximately 2 years in orbit of about 300 km in the ram direction. Figure 4 shows gravimetric mass loss measurements for TiO_2-coated Kapton and uncoated reference samples. Each titania-coated sample was accompanied by an uncoated reference Kapton sample, and the LEO equivalent AO fluence was determined by Kapton mass loss. It was observed that at high AO fluences, TiO_2-

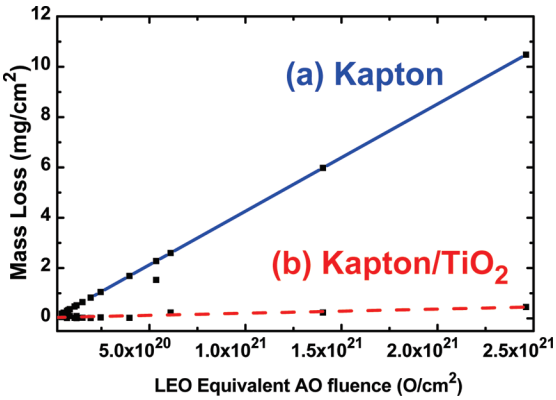

FIGURE 4. Kapton and titania-coated Kapton mass loss as a function of AO fluence.

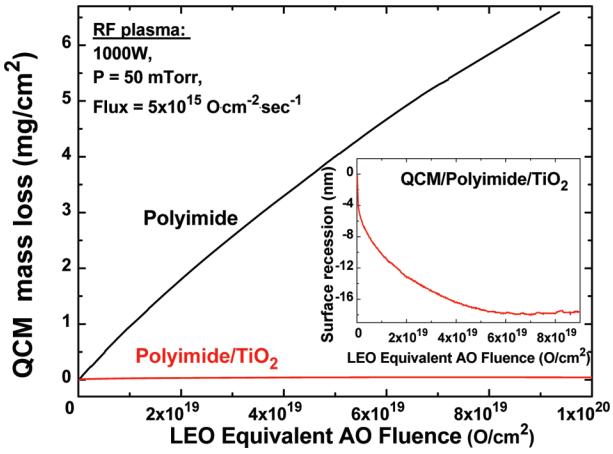

FIGURE 5. Polyimide and Polyimide/titania-coated QCM mass loss as a function of the LEO equivalent AO fluence. The inset shows surface recession of polyimide/titania-coated QCM.

coated Kapton samples were much more durable, with mass loss of only 1−2% of that of Kapton after exposure to AO fluence of 4.0×10^{20} atoms cm^{-2} and higher. Even at low fluences, the absolute values are very low compared to Kapton, as shown in Figure 4.

To study in more detail the initial stages of AO erosion, polyimide-coated QCM crystals, with or without titania protection, were used. Figure 5 shows QCM mass loss as a function of LEO-equivalent AO fluence for both reference polyimide samples and for TiO_2-coated polyimide samples. Each sample was exposed independently, under identical exposure conditions. It was observed that the mass loss of titania-coated samples is negligible when compared to the mass loss of uncoated polyimide. Nevertheless, as shown in the inset in Figure 5, some initial erosion of a very thin layer (about 18 nm) was detected. This initial mass loss may be attributed to the presence of "adventitious" carbon contamination on the surface of the coating. This is consistent with the XPS measurements reported below.

Although the improved durability of the titania-coated Kapton is seen in the reduced mass loss compared to uncoated Kapton, the surface of those AO exposed samples showed thin cracks (Figure 6). Once the cracks were formed, further AO exposure did not affect the crack density or the morphology of the film between the cracks. The width of the cracks was 50−60 nm after exposure to 1.1×10^{20} atoms cm^{-2}, and it increased to 100 nm after exposure to 3.3×10^{20} atoms cm^{-2}. Such cracks lead to undercutting of Kapton that compromises the efficiency of the protective coating. As discussed below, the appearance of cracks often indicates either (i) changes in chemical composition (oxidation) leading to surface contraction, or (ii) structural modifications/densification of the film.

3.4. Chemical Composition. The elemental composition of the TiO_2-coated Kapton was studied by XPS. Typical survey spectra of a Kapton film before and after titania deposition are shown in Figure 7. The uncoated sample shows the presence of C1s, O1s, N1s and a very weak F1s core level line. This spectrum is typical of a pristine Kapton sample. After LPD titania coating (by either method), the relative intensities of the C1s and N1s lines decrease concurrent with the appearance of Ti-related peaks (Ti2p, Ti2s, Ti3p). The increase of fluorine on the surface likely reflects residues of the $(NH_4)_2TiF_6$ (the LPD starting material) and its partial hydrolysis products. These residues may contribute to the subsequent structural changes that lead to film cracking during AO exposure.

The quantitative analysis of surface composition was carried out using detailed XPS scans of C1s, O1s, N1s, Ti2p, and F1s and standard atomic photoionization cross-section values from the SPECS database (38). The results are summarized in Table 2. As-deposited titania samples show a substantial concentration of carbon on the surface. To determine whether this carbon originates from the underlying Kapton substrate or from adventitious carbon contamination of the coated surface, the TiO_2-coated sample was subjected to Ar^+ ion sputtering. It was observed that the carbon concentration decreased very quickly with sputter time. From sputter rate calibration it was estimated that there is about 10−15 nm of so-called adventitious carbon, which is in a good agreement with the QCM results (Figure 5). The amount of adventitious carbon appears to be lower in the case of titania coating deposited by method II, but it is likely that this is of no consequence.

The XPS measurements showed minimal changes in the elemental composition of the coating after AO exposure, especially for coating deposited by method I. The O1s peak was deconvoluted into two components, representing Ti−O (533.5 eV) and O−H or O−C (535.1 eV). The ratio of oxygen-to-titanium (as Ti−O peak) showed minimal change, from 2.2 to 2.3 in the case of method I, and a slightly higher change, from 2.3 to 2.5, in the case of method II. The changes observed in the carbon content and in nontitania oxygen (O−H or O−C) may be explained by losses of adventitious carbon and postexposure water adsorption, respectively.

3.5. Mechanical Properties. Mechanical properties of Kapton with and without deposited TiO_2 films, before and after AO exposure, were assessed by AFM nanoindentation measurements. Surface hardness was obtained from nanoindentation force-displacement curves generated using loading and unloading cycles. To avoid substrate effects on the

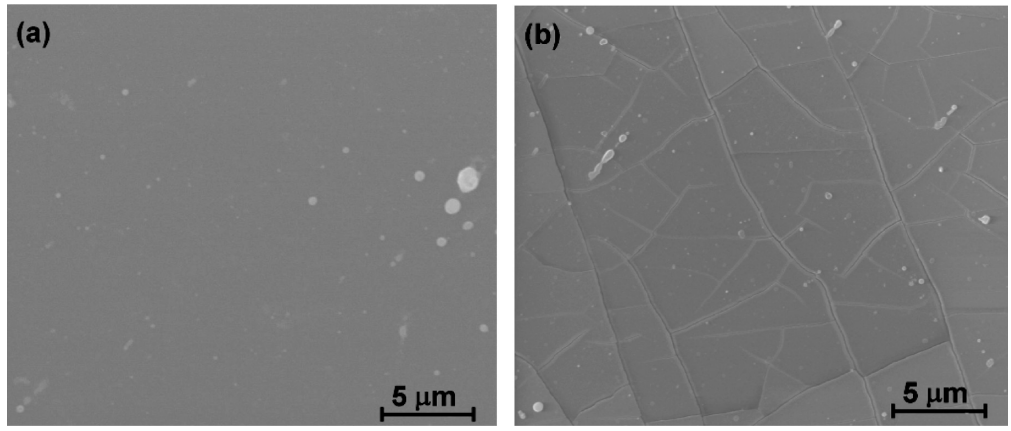

FIGURE 6. ESEM images of titania-coated Kapton sample before (a) and after (b) exposure to 1.5×10^{19} atoms cm^{-2} AO fluence.

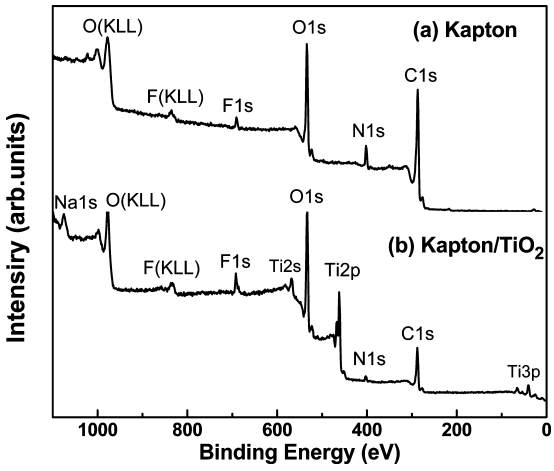

FIGURE 7. XPS survey scans of a reference Kapton film (a) before and (b) after LPD titania coating.

measured hardness of the coating, the applied load was set for an indentation depth of only a few tens of nanometers (less than half the thickness of the coating). Measurement procedures and calculation methods are described elsewhere (39). The hardness of uncoated Kapton is about 0.2 GPa. For titania-coated samples, the hardness is at least an order of magnitude higher (2.3 GPa). These values are comparable with the published hardness values for titania and Kapton (40–43). A hardness value similar to that of titania was also measured for AO-exposed titania-coated Kapton, indicating that AO does not affect the hardness of the protective coating. It should be noted that the calculated hardness values were obtained for the bulk of the coating, about 50−100 nm below the surface. This is consistent with the idea that AO exposure, which affects only the top surface layer, does not change the mechanical properties of the film. The effect of AO on the top surface layer is demonstrated by the scratch tests described below.

The titania-coated samples were scratch-tested using a diamond-tipped cantilever for nanoindenting/scratching. Figure 8 shows an AFM image of the titania-coated Kapton after scratching with a normal force of 6 μN. The scratch groove depths are summarized in Table 3. Each value represents an average of three measurements under similar load conditions. An uncoated Kapton reference sample shows a deepest scratch groove of about 9 nm. Titania coating does not significantly affect this value, and a scratch groove of 8 nm can be obtained. Exposure of the titania-coated Kapton to AO fluence of $2-3 \times 10^{20}$ atoms cm^{-2} leads to a shallower scratch groove (~2 nm), indicating a change in the mechanical properties of the surface layer. This would be consistent with a densification of the titania coating due to VUV radiation effects, as discussed below.

3.6. Thermo-Optical Properties. Thermo-optical properties (solar absorptance α_s and thermal emmitance ε) of Kapton and of titania-coated Kapton samples before and after AO exposure were measured (Table 4). Titania coatings prepared by method I do not affect the α_s/ε ratio, so that the value for Kapton ($\alpha_s/\varepsilon = 0.507$) is maintained ($\alpha/\varepsilon = 0.506$). The coating produced by method II gives a higher α_s/ε ratio compared to uncoated Kapton (0.757 compared to 0.507). After AO exposure, the α_s/ε ratio of all samples increases. For uncoated Kapton the increase is the highest (25%), while for titania-coated Kapton prepared by method I the increase is the lowest (only 11%). The titania deposited by method II results in a 20% increase of α_s/ε after exposure to a very low AO fluence of 5×10^{19} atoms/cm^2.

3.7. Electrostatic Properties. EFM images were recorded using electrostatic tips and a tapping/lift mode with a MultiMode SPM (44). In tapping/lift mode, both the topography and electrostatic contrast are measured simultaneously. The sample surface is scanned twice, repeating each scanned line in both modes. In the first scan the surface is detected in the standard tapping mode while measuring the surface morphology. In the second scan the topographic data are used to retrace the first scan, while the tip keeps a constant height (up to 100 nm) above the surface. During the second scan, the tip is oscillated at its free resonance frequency and a DC bias voltage is applied between the tip and the samples. The electrical field formed by the applied DC bias voltage will create surface electrical charges which, in turn, create a corresponding electrical field that affects the tip's frequency. A phase difference between the resonance frequency and the observed frequency of the tip is measured (45). An EFM image, based on the phase difference, reflects the charge distribution on the sample surface (46).

Table 2. Surface Elemental Composition (at %) Based on XPS Analysis

	C	O total/Ti−O/(O−H, O−C)	Ti	F	N	$O_{(Ti-O)}$/Ti
Kapton (plasma pretreatment)	66.7	22/0/22		0.9	7.5	
method I, as deposited	29.1	46.9/41.0/5.9	18.6	3.8	1.5	2.2
method I, AO (3×10^{19} atoms cm^{-2})	16.7	56.7/44.2/12.5	19.5	5.7	1.2	2.3
method II, as deposited	19.2	50.6/42.6/8.0	18.8	8.7	2.6	2.3
method II, AO (5×10^{19} atoms cm^{-2})	18.6	55.0/36.9/18.1	14.9	5.2	1.9	2.5

Figure 9 shows AFM and EFM images of titania-coated Kapton (method I). The EFM images (Figure 9b−d) were taken in a lift mode at 50 nm tip−surface distance and tip biases of 0, 2, and 5 V, respectively. For comparison, a morphology image (Figure 9a) taken using tapping AFM mode is also shown. A lift height of 50 nm is sufficient to prevent any topographical effects. Therefore, any surface structuring that appears in Figure 9b−d is related to electrical charging. Titania is a wide band gap semiconductor (E_g = 3.25−3.33 eV). Thus, the tip bias of 0 V did not result in any surface charging and, accordingly, no features are visible. A bias of 2 V is below the band gap value of titania and no charging is expected. However, Figure 8c reveals subtle surface structures. The surface charging could originate from charge carrier mobility due to either intermediate states in the band gap, or humidity on the surface. At a tip bias of 5 V (greater than the band gap), surface charging is evident. The surface charging generates electrostatic forces, which lead to an EFM contrast map that is identical to the surface morphology (compare images a and d in Figure 9). This indicates that the titania coating possesses sufficient electrical conductivity to prevent electrostatic discharge problems.

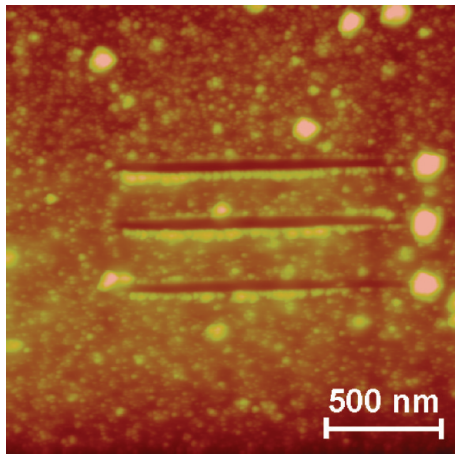

FIGURE 8. AFM images of scratch grooves on titania-coated Kapton (method I). The image size is 5 × 5 μm; image height 100 nm.

Table 3. Scratch Test Results

sample	scratch groove depth (nm)
Kapton	9.3
Kapton/TiO_2 (method I)	8.0
Kapton/TiO_2 (method I) 2×10^{20} atoms cm^{-2}	2.4
Kapton/TiO_2 (method I) 3×10^{20} atoms cm^{-2}	2.3

Table 4. Thermo-Optical Properties (α_s, ε, α/ε)

sample	α_s	ε	α_s/ε
Kapton	0.426	0.840	0.507
Kapton/AO (1×10^{20} O/cm^2)	0.538	0.850	0.634
Kapton/TiO_2 (method I)	0.422	0.833	0.506
method I 1.5×10^{20} atoms/cm^2	0.483	0.860	0.562
Kapton/TiO_2 (method II)	0.645	0.852	0.757
method II, 5×10^{19} atoms/cm^2	0.820	0.902	0.909

4. DISCUSSION

Spacecraft in the LEO environment are exposed to hazards that can degrade the properties of outer surfaces. The main effects of the LEO environment arise from AO, UV radiation, hypervelocity debris impact and ESD. Outer surfaces composed of polymers such as Kapton require protection against these hazards. A common protective layer is a vacuum-deposited ceramic coating, e.g., SiO_2 or ITO. The results reported above suggest an alternative, simple, low-cost method of ceramic coating that can address many of these problems. Two procedures for the LPD of titania thin films on Kapton are described: method I (room temperature, pH 3.88) provides 100 nm thick films of amorphous titania, whereas method II uses a more acidic solution (pH 2.88) at 50 °C and leads to thicker, largely crystalline, films (300−400 nm) (30).

Space durability of a coating is assessed by a combination of (i) AO erosion yield (mass loss); (ii) changes in chemical composition due to oxidation and/or etching reactions; (iii) morphological changes and surface cracking; (iv) changes in thermo-optical properties (α/ε); (v) changes in mechanical properties; and (vi) the capability to prevent electrostatic discharge. These issues have all been examined.

Both LPD techniques (method I and method II) provide coatings with high AO protection efficiency, resulting in a negligible mass loss. XPS shows that in both cases the top-surface layer is comprised largely of titanium dioxide (TiO_2), contaminated by small amounts of hydrocarbon, hydroxyl groups and fluoride. Titania deposited by method II (largely crystalline) shows a modest increase in the O/Ti ratio after AO exposure. This may be due to the formation of peroxide-like Ti−O−O− groups (47). The amount of increased oxygen is small and does not seem to affect the barrier properties of the coating.

The cracking of the coating observed after exposure to simulated AO environment seems not to be related to changes in the chemical composition of the oxide film, but rather to changes in film structure. The structure of the titania may be affected by the exposure environment, especially by the VUV radiation, which accompanies the AO exposure in the RF plasma-based simulation facilities (as well as in LEO). A restructuring of the titania might lead to density

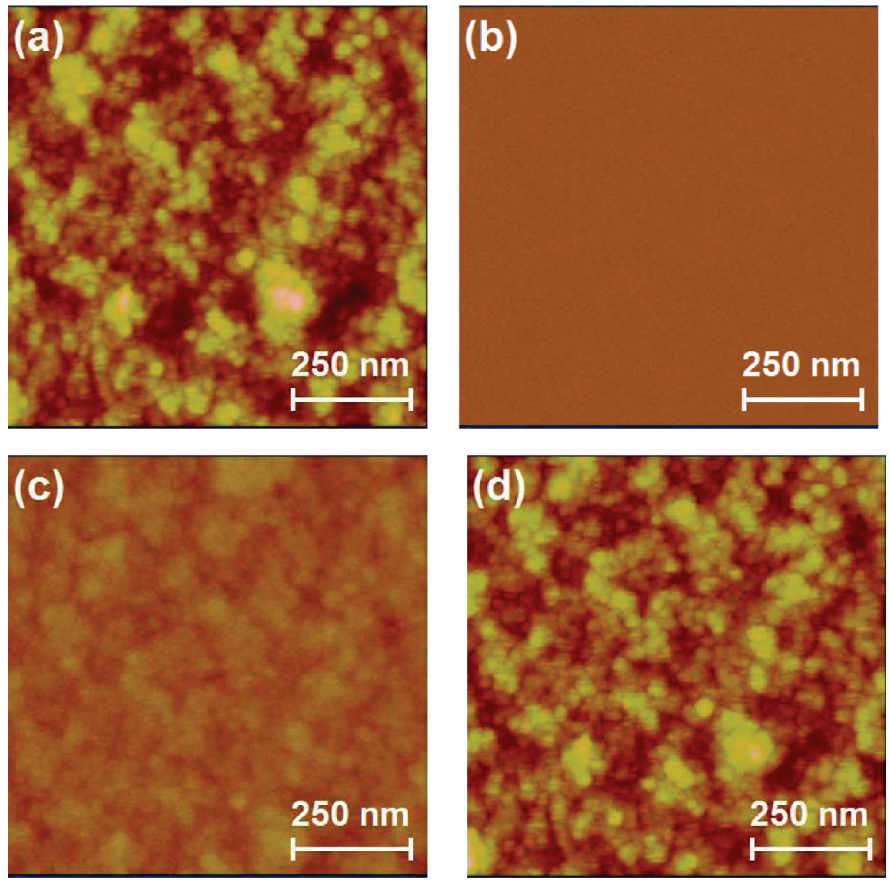

FIGURE 9. AFM and EFM images of titania-coated Kapton (method I). (a) Morphology image taken by tapping AFM mode, EFM images taken in a lift mode at 50 nm tip−surface distance and tip bias of (b) 0 V, (c) 2 V, and (d) 5 V. Height scale is (a) 25 nm and (b−d) 5°.

changes in the coating, which would produce stresses and, eventually, cracking of the surface. This speculation is supported by other reports of crystallization and densification of sol−gel derived titania films exposed to VUV irradiation (48, 49) and by the results of the scratching test. Nakajima et al. (48) reported that VUV illumination (2 h) of a sol−gel-based TiO_2 film using a Xe excimer lamp (172 nm wavelength) resulted in its densification and a lessening in film thickness from 290 to 146 nm. It was explained by photo-induced removal of OH groups and organic contamination. This mechanism could be applicable also in the case of LPD titania films; however, further studies, mainly the exposure of the films to VUV irradiation alone, are needed to verify this hypothesis. It should be emphasized, however, that in spite of possible structural modifications and cracking of the surface, the AO erosion of titania-coated Kapton film after exposure to AO fluence of 4.0×10^{20} atoms cm^{-2} and higher, was about 2 orders of magnitude lower than that of pristine Kapton.

Operating in a vacuum presents challenges in preventing heat build-up within the components onboard a spacecraft. Thermal balance is controlled mainly by the thermo-optical properties of the outer surfaces. Optimal properties include low solar absorbance (α_s) and high thermal emittance (ε). Suitable thermo-optical properties are defined by a low α_s/ε ratio. Kapton provides appropriate thermo-optical properties for space usage, with $\alpha_s/\varepsilon = 0.5$ (see Table 4). This value can be changed because of interaction with the space environment. For instance, uncoated Kapton exposed to LEO on the Long Duration Exposure Facility (LDEF) satellite showed an increase of up to 16% in α_s/ε value (1).

Titania coatings deposited by method I did not affect the initial value of α_s/ε measured for Kapton. Exposure to AO increased the α_s/ε of a method I titania coating by 11%, a significantly smaller change than that observed for uncoated Kapton (25%). The coating produced by Method II was characterized by a higher initial α_s/ε value (0.76), and this value increased by 20% after AO exposure. The mechanism of thermo-optical changes following exposure to simulated AO environment is not totally understood. In general, changes in surface morphology, mainly surface roughness, might modify the α_s/ε ratio (50). In addition, the presence of UV radiation might also affect the thermo-optical properties of titanium oxide by formation of color centers due to photoinduced oxygen vacancies (51). Oxygen vacancies were shown to be responsible for yellowing titania films (52). Titania films produced by method II showed a larger increase in the α_s/ε value, 20%, compared to 11% observed in films produced by method I. The difference is attributed to the films' thicknesses. Films produced by method II are thicker than those produced by method I, leading to a greater effect on the α_s/ε value. Either way, it renders the method II coatings somewhat less appropriate for the protection tasks addressed herein.

Spacecraft orbiting in LEO are exposed to electrical discharge, originating from two major sources: space plasma

and photoemission currents. The possibility of electrically charging external surfaces requires a LEO protective coating that is capable of preventing ESD, especially for spacecraft in polar orbit. EFM measurements reveal that applying low voltages (of about 5 V) leads to mobility of surface charge carriers. This result speaks to the antistatic properties of the titania coating and could make it suitable for preventing ESD.

5. CONCLUSIONS

The present work shows that LPD is a promising, simple, non-line-of-sight limited, low-cost, water-based method for protecting Kapton from the LEO environment. Uniform films of titania have been prepared at near-ambient conditions. These films possess very attractive properties for space applications. They provide protection against AO exposure, with erosion yield of 2% of that measured for unprotected Kapton. Due to VUV radiation, originating from RF-based simulation facility, the titania coating showed minor cracking, a phenomena that had no effect on the measured mass loss. The as-deposited coating (particularly the amorphous titania of method I) largely maintained the required thermo-optical properties after AO irradiation. The AO attack did not alter the chemical composition of the coatings, although it did slightly improve their mechanical properties. Titania, being a wide band gap semiconductor, also seems to be capable of preventing ESD problems.

Acknowledgment. This research was supported in part by the Israeli Ministry of Science and by the Edward and Judy Steinberg Chair in Nanotechnology at Bar Ilan University.

REFERENCES AND NOTES

(1) Silverman, E. M. *Space Environmental Effects on Spacecraft—LEO Material Selection Guide*; NASA Contractor Report No. 4661.; Langley Research Center, National Aeronautics and Space Administration: Langley, VA,1995.
(2) Tribble, A. C., *The Space Environment: Implementation for Spacecraft Design*; Princeton University Press: Princeton, NJ, 1995.
(3) Bedingfield, K. L.; Leach, R. D.; Alexander, M. B. *Spacecraft System Failures and Anomalies Attributed to the Natural Space Environment*; NASA Reference Publication 1390; National Aeronautics and Space Administration: Washington, D.C., 1996.
(4) Minton, T. K.; Garton, D. J., Dynamics of Atomic-Oxygen-Induced Polymer Degradation in Low Earth Orbit. In *Chemical Dynamics in Extreme Environments*; Dressler, R. A., Ed; Advanced Series in Physical Chemistry; World Scientific: Singapore, 2001; pp 420—489.
(5) *Standard Practices for Ground Laboratory Atomic Oxygen Interaction Evaluation of Materials for Space Applications*; American Society for Testing and Materials: West Conshohocken, PA, 2000.
(6) Buczala, D. M.; Brunsvold, A. L.; Minton, T. K. *J. Spacecr.Rockets* **2006**, *43*, 421–425.
(7) Zimcik, D. G.; Wertheimer, M. R.; Balmain, K. B.; Tennyson, R. C. *J. Spacecr. Rockets* **1991**, *28*, 652–657.
(8) Reddy, R. M. *J. Mater. Sci.* **1995**, *30*, 281–307.
(9) Kleiman, J. I.; Gudimenko, Y.; Ng, R.; Iskanderova, Z. A.; Grigorevski, A.; Kiseleva, L.; Edwards, D.; Finckenor, M. *J. Spacecr. Rockets* **2006**, *43*, 443–450.
(10) Iskanderova, Z. A.; Kleiman, J. I.; Gudimenko, Y.; Tkachenko, A.; Tennyson, R. C.; Brown, I. G.; Monteiro, O. R. *Nucl. Instrum. Methods Phys. Res., Sect. B* **1999**, *148*, 1090–1096.
(11) Gudimenko, Y.; Ng, R.; Kleiman, J.; Iskanderova, Z.; Milligan, D.; Tennyson, R. C.; Hughes, P. C. *J. Spacecr. Rockets* **2004**, *41*, 326–334.
(12) Brunsvold, A. L.; Minton, T. K.; Gouzman, I.; Grossman, E.; Gonzalez, R. *High Perform. Polym.* **2004**, *16*, 303–318.
(13) Verker, R.; Grossman, E.; Gouzman, I.; Eliaz, N. *High Perform. Polym.* **2008**, *20*, 475–491.
(14) Rutledge, S. K.; Mihelcic, J. A. *Surf. Coat. Technol.* **1989**, *39—40*, 607.
(15) Herrero, J.; Guillén, C. *Vacuum* **2002**, *67*, 611.
(16) Bauer, E. G.; Dodson, B. W.; Ehrlich, D. J.; Feldman, L. C.; Flynn, C. P.; Geis, M. W.; Harbison, J. P.; Matyi, R. J.; Peercy, P. S. *J. Mater. Res.* **1990**, *5*, 852.
(17) Phule, P. P.; Risbud, S. H. *J. Mater. Sci.* **1990**, *25*, 1169.
(18) Cooper, R.; Upadhyaya, H. P.; Minton, T. K.; Berman, M. R.; Du, X.; George, S. M. *Thin Solid Films* **2008**, *516*, 4036.
(19) George, S. M. *Chem. Rev.* **2009**, *110*, 111.
(20) Deki, S.; Aoi, Y.; Hiroi, O.; Kajinami, A. *Chem. Letters.* **1996**, 433.
(21) Deki, S.; Aoi, Y.; Miyake, Y.; Gotoh, A.; Kajinami, A. *Mater. Res. Bull.* **1996**, *31*, 1399–1406.
(22) Pizem, H.; Gershevitz, O.; Goffer, Y.; Frimer, A. A.; Sukenik, C. N.; Sampathkumaran, U.; Milhet, X.; McIlwain, A.; De Guire, M. R.; Meador, M. A. B.; Sutter, J. K. *Chem. Mater.* **2005**, *17*, 3205.
(23) Pizem, H.; Sukenik, C. N.; Sampathkumaran, U.; McIlwain, A. K.; De Guire, M. R. *Chem. Mater.* **2002**, *14*, 2476–2485.
(24) Razgon, A.; Sukenik, C. N. *J. Mater. Res.* **2005**, *20*, 2544–2552.
(25) Hatanaka, Y.; Naito, H.; Itou, S.; Kando, M. *Appl. Surf. Sci.* **2005**, *244*, 554.
(26) Glassford, K. M.; Chelikowsky, J. R. *Phys. Rev. B* **1992**, *46*, 1284.
(27) DeLoach, J. D.; Scarel, G.; Aita, C. R. *J. Appl. Phys.* **1999**, *85*, 2377.
(28) Martin, N.; Rousselot, C.; Rondot, D.; Palmino, F.; Mercier, R. *Thin Solid Films* **1997**, *300*, 113–121.
(29) Jellison, J. G. E.; Boatner, L. A.; Budai, J. D.; Jeong, B. S.; Norton, D. P. *J. Appl. Phys.* **2003**, *93*, 9537.
(30) Girshevitz, O.; Silickas, P.; Sukenik, C. N. Modification and coating of polymer surfaces. In *Surface Chemistry in Biomedical and Environmental Science*; Blitz, J. P., Gun'ko, V. M., Eds.; Springer: Dordrecht, The Netherlands, 2006; pp 59—68.
(31) Koumoto, K.; Seo, S.; Sugiyama, T.; Seo, W. S.; Dressick, W. J. *Chem. Mater.* **1999**, *11*, 2305.
(32) Briggs, D.; Seah, M. P. *Practical Surface Analysis. Auger and X-ray Photoelectron Spectroscopy*, 2nd ed.; John Wiley & Sons: Chichester, U.K., 1992; Vol. 1, p 533.
(33) Doolittle, L. R. *Nucl. Inst. Methods Phys. Res., Sect. B* **1986**, *15*, 227–231.
(34) Shpilman, Z.; Gouzman, I.; Lempert, G.; Grossman, E.; Hoffman, A. *Rev. Sci. Instrum.* **2008**, *79*, Art. no. 025106.
(35) De Groh, K. K.; Banks, B. A.; McCarthy, C. E.; Rucker, R. N.; Roberts, L. M.; Berger, L. A. *High Perform. Polym.* **2008**, *20*, 388–409.
(36) *PYRALIN Polyimide Coating PI 2545 PI 2540 Product Information*; DuPont. Inc., Technical Bulletin; DuPont: Wilmington, DE, February 1993.
(37) Verker, R.; Grossman, E.; Gouzman, I.; Eliaz, N. *Compos. Sci. Technol.* **2009**, *69*, 2178–2184.
(38) *CasaXPS VAMAS Processing Software*; available from http://www.casaxps.com/.
(39) Laikhtman, A.; Gouzman, I.; Verker, R.; Grossman, E.; Pippin, H. G. *High Perform. Polym.* **2008**, *20*, 447–4609833010.
(40) Zywitzki, O.; Modes, T.; Sahm, H.; Frach, P.; Goedicke, K.; Glow, D. *Surf. Coat. Technol.* **2004**, *180—181*, 538–543.
(41) Latella, B. A.; Gan, B. K.; Li, H. *Surf. Coat. Technol.* **2007**, *201*, 6325–6331.
(42) Kern, P.; Schwaller, P.; Michler, J. *Thin Solid Films* **2006**, *494*, 279–286.
(43) Kucheyev, S. O.; Felter, T. E.; Anthamatten, M.; Bradby, J. E. *Appl. Phys. Lett.* **2004**, *85*, 733–735.
(44) Hong, J. W.; Khim, Z. G.; Hou, A. S.; Park, S. I. *Appl. Phys. Lett.* **1996**, *69*, 2831–2833.
(45) Lee, Y.; Kang, M. *Mater. Chem. Phys.* , *122*, 284–289.
(46) Albrecht, T. R.; Grutter, P.; Horne, D.; Rugar, D. *J. Appl. Phys.* **1991**, *69*, 668–673.
(47) Pashkova, A.; Svajda, K.; Black, G.; Dittmeyer, R. *Rev. Sci. Instrum.* **2009**, *80*, 055104.
(48) Nakajima, A.; Hayashi, N.; Taniguchi, Y.; Kameshima, Y.; Okada, K. *Surf. Coat. Technol.* **2005**, *192*, 112–116.
(49) Nanjo, H.; Xia, Z.; Yao, Y.; Minami, K.; Nishioka, M. *e-J. Surf. Sci. Nanotechnol.* **2005**, *3*, 284–293.
(50) Shimamura, H.; Miyazaki, E. *J. Spacecr. Rockets* **2009**, *46*, 241–247.
(51) Kuznetsov, V. N.; Serpone, N. *J. Phys. Chem. C* **2007**, *111*, 15277–15288.
(52) Sekiya, T.; Ichimura, K.; Igarashi, M.; Kurita, S. *J. Phys. Chem. Solids* **2000**, *61*, 1237–1242.

AM100113T